ACS APPLIED NANO MATERIALS
Cite This: ACS Appl. Nano Mater. 2018, 1, 4548−4556
Article
www.acsanm.org

Evaluation of Thermal and Radiation Induced Chemistries of Metal Oxo−Hydroxo Clusters for Next-Generation Nanoscale Inorganic Resists

Richard P. Oleksak,[†] Rose E. Ruther,[†,‡] Feixiang Luo,[§] Jennie M. Amador,[‡] Shawn R. Decker,[‡] Milton N. Jackson,[∥] Joshua R. Motley,[†] Jason K. Stowers,[‡] Darren W. Johnson,[*,∥] Eric L. Garfunkel,[*,§] Douglas A. Keszler,[*,‡] and Gregory S. Herman[*,†]

[†]School of Chemical, Biological and Environmental Engineering and [‡]Department of Chemistry, Oregon State University, Corvallis, Oregon 97331, United States

[§]Department of Chemistry and Chemical Biology, Rutgers University, Piscataway, New Jersey 08854, United States

[∥]Department of Chemistry and Biochemistry & Materials Science Institute, University of Oregon, Eugene, Oregon 97403-1253, United States

ABSTRACT: Thin films formed by the condensation of metal oxo−hydroxo clusters offer a promising approach to ultrahigh-resolution patterning including next-generation photolithography using extreme ultraviolet (EUV) radiation and electron-beam lithography. In this work, we elucidate the thermal and radiative mechanisms that drive the chemical transformations in these materials and therefore control the patterning performance. Beginning from aqueous hafnium clusters, peroxide and sulfate additions serve to modify the clusters and, upon spin coating to form a thin film, provide the chemical contrast necessary to create resist. The coordination and functionality of peroxide and sulfate in hafnium-based metal oxo−hydroxo clusters were monitored at various stages of the patterning process which provided insight into the chemical and structural evolution of the material. Peroxide serves as the radiation sensitive species while sulfate enhances solubility and controls the concentration of hydroxide in the films. Peroxide and hydroxide species decompose via radiative and thermal energy, respectively, to form hafnium oxide; controlling these processes is central to the function of the resist.

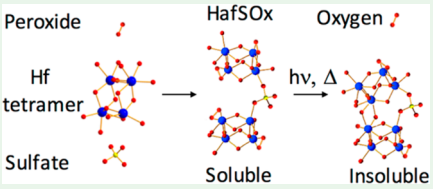

KEYWORDS: *nanopatterning, lithography, cluster, polyoxometalate, metal oxide photoresist, inorganic photoresist*

■ INTRODUCTION

Metal oxo−hydroxo clusters[1] are among the smallest building blocks in nature and ideal precursors for the design of structures approaching the atomic scale. The patterning of such features at the smallest possible size has largely driven performance in many technological applications. One approach to accomplish this is through the process of lithography—a practice which dates to the late 1700s and today forms the cornerstone of nanoscale fabrication processes and the $1 trillion consumer electronics industry.

Lithography is the practice of creating 2-dimensional thin film structures through a multiple-step patterning process.[2] First, a precursor solution is used to deposit a thin film of radiation-sensitive resist material onto a thin film or substrate to be patterned. A modest heat treatment is used to drive off excess solvent, and the material is partially exposed to radiation (photons or electrons), where a chemical transformation leads to a solubility change in the exposed regions. The resist is developed by dissolving the exposed (or unexposed) regions in a suitable solvent, leaving a pattern of etch resistant material. This pattern is transferred to the underlying thin film or substrate by etching, the residual resist is removed, and this process is repeated many times to build thin film 2- or 3-dimensional structures. The performance of this patterning process is measured by three key parameters: resolution (the smallest length scale where a repeatable pattern is possible), sensitivity (the exposure energy required to drive the solubility switch), and line edge roughness (LER).[3] Resolution and LER limit the smallest achievable feature size, while sensitivity determines the speed at which patterned structures may be written using photolithographic processes.

The achievable patterning performance is integrally related to both the photoresist and the radiation source. Chemically amplified photoresists have been widely used since their introduction in the 1980s. These materials are exposed using deep ultraviolet (DUV) radiation, for example by an ArF excimer laser (λ = 193 nm). These photoresists display exceptional sensitivity; however, factors such as long acid diffusion lengths and statistical dose fluctuations result in large LER and limit spatial resolution.[4] Much higher resolutions have been demonstrated using nonchemically amplified resists including poly(methyl methacrylate) (PMMA)[5,6] and hydrogen silsesquioxane (HSQ);[7,8] however, these materials have poor sensitivity. As technological advances continue to drive

Received: May 23, 2018
Accepted: August 20, 2018
Published: August 20, 2018

Downloaded via RUTGERS UNIV on January 1, 2019 at 22:55:17 (UTC).
See https://pubs.acs.org/sharingguidelines for options on how to legitimately share published articles.

ACS Publications © 2018 American Chemical Society

DOI: 10.1021/acsanm.8b00865
ACS Appl. Nano Mater. 2018, 1, 4548−4556

Lam Research Ex. 1019 - Page 1
Lam Research Corp. v. Inpria Corp.
IPR2024-00033 - U.S. Patent No. 9,823,564

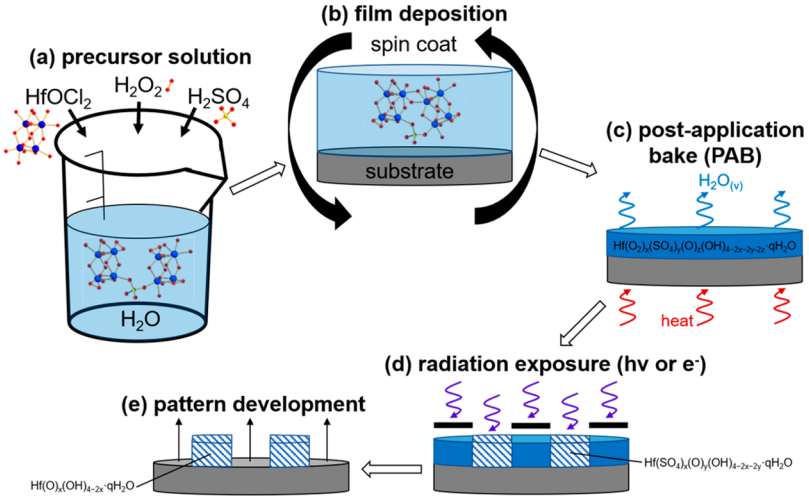

Figure 1. Summary of the HafSOx patterning process, which is discussed in detail throughout the paper. (a) Precursor solution is formed by combining $HfOCl_2$, H_2O_2, and H_2SO_4 in deionized water. These provide a source of Hf tetramers ($[Hf_4(OH)_8(H_2O)_{16}]^{8+}$), peroxide ions ($O_2^{2-}$), and sulfate ions ($SO_4^{2-}$). (b) Films are deposited by spin coating. (c) A postapplication bake (PAB) removes excess water. (d) Films are exposed to radiation (photons or electrons) resulting in a solubility decrease in the exposed regions. (e) The pattern is developed by dissolving unexposed regions in a suitable solvent.

pattern dimensions to smaller length scales, the structure of the fundamental units comprising the photoresist becomes significant. Large LER in polymer-based photoresists can be attributed to the formation of polymer aggregates tens of nanometers in size.[9−11] Advances in obtaining low LER in photoresists based on calixarene,[12] molecular glasses,[13] HSQ,[14] and nanoparticles[15] are likely related to the small size and uniformity of the nanoscale units which comprise these materials. The development of photoresists based on ultrasmall precursors offers a promising approach to continued improvements in patterning resolution; however, sensitivity limitations must be addressed, especially when moving beyond DUV.

The maximum achievable patterning resolution scales with the wavelength of the radiation source. While DUV sources have been used for patterning features at dimensions well below the corresponding wavelength (λ = 193 nm) by using techniques such as immersion lithography and multiple patterning, improvements made possible by these modifications are limited and new radiation sources will be required for further advances in patterning resolution, especially for dense arrays of features <10 nm. Extreme ultraviolet (EUV) has been identified as the most promising next-generation radiation source with λ = 13.5 nm.[16] A primary barrier to EUV photolithography is the relatively low power output of current EUV light sources, limiting throughput. Furthermore, conventional polymer-based photoresists that demonstrate high sensitivity at DUV wavelengths exhibit low absorption at EUV. Next-generation photoresists must be designed to achieve not only ultrahigh resolution but also high sensitivity to EUV radiation.

Metal oxo−hydroxo clusters are discrete structures on the order of 1 nm or smaller, characterized by significant metal−oxygen bonding. These species offer a promising approach to ultrahigh resolution patterning, for example, using photolithography at EUV wavelengths and beyond,[17] as highly monodisperse clusters can be synthesized and used to produce nearly atomically smooth films with cluster sizes well below what is typically achieved with other methods. Furthermore, many transition metals exhibit very high EUV absorption and clusters based on these materials may lead to high sensitivity in the final photoresist. Extremely smooth films have been demonstrated for metal oxo−hydroxo clusters, with the nominal composition $Hf(SO_4)_y(O)_z(OH)_{4-2y-2z}{\cdot}qH_2O$.[18] By further functionalizing the precursor solution with peroxide, the nominal film composition changes to $Hf(O_2)_x(SO_4)_y(O)_z(OH)_{4-2x-2y-2z}{\cdot}qH_2O$ (HafSOx), and the radiation sensitive peroxide ligand provides the chemical contrast necessary to create a photoresist.[19] As a photo or electron beam (e-beam) resist, HafSOx has demonstrated high resolution patterning with relatively high sensitivity and very low LER.[19−23] Recent studies on a similar commercial hafnium/peroxide/sulfate based resist have demonstrated high resolution patterning down to 7 nm using EUV, which may enable the 2.5 nm technology node.[24] While the mechanisms governing the patternability of HafSOx[25,26] and other oxide-based resists[27−30] have been postulated, direct evidence leading to a fundamental understanding of these mechanisms has not been adequately achieved.

In this contribution, we investigate the patterning process of the HafSOx system (illustrated schematically in Figure 1) and explore the path from aqueous metal oxo−hydroxo cluster to dense metal-oxide nanopattern.

In revealing this path, we advance understanding of the detailed mechanism of an inorganic oxide-based resist and provide the foundation for advancing nanoscale patterning using metal oxo−hydroxo clusters.

■ RESULTS AND DISCUSSION

Understanding the patterning process begins with the precursor solution. A HafSOx solution is formed by the sequential addition of aqueous $HfOCl_2$, H_2O_2, and H_2SO_4. Hafnium forms tetranuclear clusters of stoichiometry $[Hf_4(OH)_8(H_2O)_{16}]^{8+}$ in low pH aqueous solutions free of strongly complexing anions, such as $HfOCl_2(aq)$.[31,32] The structure of these clusters is shown in Figure 2a.

Each Hf atom is bound to four bridging hydroxide O atoms and four terminal water O atoms. This tetranuclear hafnium cluster constitutes the core building block from which nanoscale patterns are eventually derived. Both peroxide and

DOI: 10.1021/acsanm.8b00865
ACS Appl. Nano Mater. 2018, 1, 4548−4556

Lam Research Ex. 1019 - Page 2
Lam Research Corp. v. Inpria Corp.
IPR2024-00033 - U.S. Patent No. 9,823,564

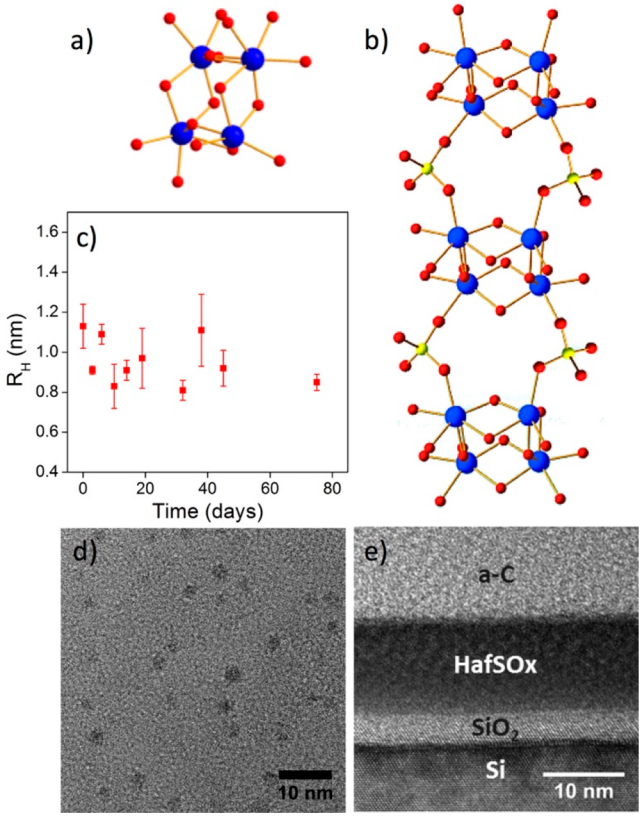

Figure 2. (a) Structure of hafnium tetramer (blue spheres are Hf and red spheres are O). (b) Hafnium tetramers linked by bridging sulfate groups (yellow spheres are S). (c) Time-dependent DLS analysis of a 150 mM HafSOx solution. (d) TEM image of isolated and linked HafSOx clusters deposited on a grid. (e) TEM image showing the cross section of a HafSOx film spin-coated on a Si substrate with a native oxide (SiO_2) layer. An amorphous carbon layer (a-C) was deposited to protect the surface during sample preparation..

sulfate are known to strongly coordinate to hafnium(IV)[33] and serve to modify the predominant metal oxo−hydroxo cluster species in solution. Peroxide acts as a capping ligand, stabilizing the Hf tetramer[34] and preventing significant polymerization of clusters in solution. The addition of sulfate in the absence of peroxide results in the precipitation of the solution species in less than 1 h. In the presence of Hf tetramers stabilized by peroxide, sulfate acts as a bridge, linking tetramers into short chains as schematically shown in Figure 2b.[34] As shown by the time-dependent DLS analysis in Figure 2c, these clusters have a hydrodynamic radius of ≈1 nm and are stable for months or more when stored at low temperature (5 °C) to inhibit the thermal decomposition of peroxide.

The HafSOx precursor was further characterized by evaporating a small volume of solution onto a grid and imaging with a TEM (Figure 2d). Clusters ranging from approximately 2 to 5 nm were observed with the highest frequency; however, clusters as small as sub-1 nm have also been observed.[35] The larger cluster size seen by TEM relative to DLS suggests that some polymerization of clusters has occurred during evaporation onto the TEM grid. Thus, the TEM results confirm the HafSOx precursor solutions consist of nanometer-sized species and provide the first insight into the polymerization of clusters during the transition from the solution to solid state. During spin-coating, clusters in the HafSOx precursor solutions are rapidly assembled to form a dense and uniform film as shown in Figure 2e. This cross-sectional TEM image illustrates the very smooth surface of the film, which is related to the small cluster sizes in the precursor solution. Atomic force microscopy (AFM) measurements were used to confirm very low root-mean-square (RMS) roughness values for the films, which ranged from 0.15 to 0.19 nm. The surface roughness of photoresists has been correlated to LER in fully developed patterns,[10,11,14] and thus the extreme smoothness of HafSOx films leads to the exceptionally low LER observed in the patterned films.[19,20]

Raman spectroscopy was used to track the coordination of peroxide and sulfate to the hafnium clusters during the transition from solution to film. Raman spectra of the HafSOx precursor solution and the resulting HafSOx thin films formed with and without the peroxide ligand species are shown in Figure 3a. Spectra for sulfuric acid and hydrogen peroxide are provided for comparison.

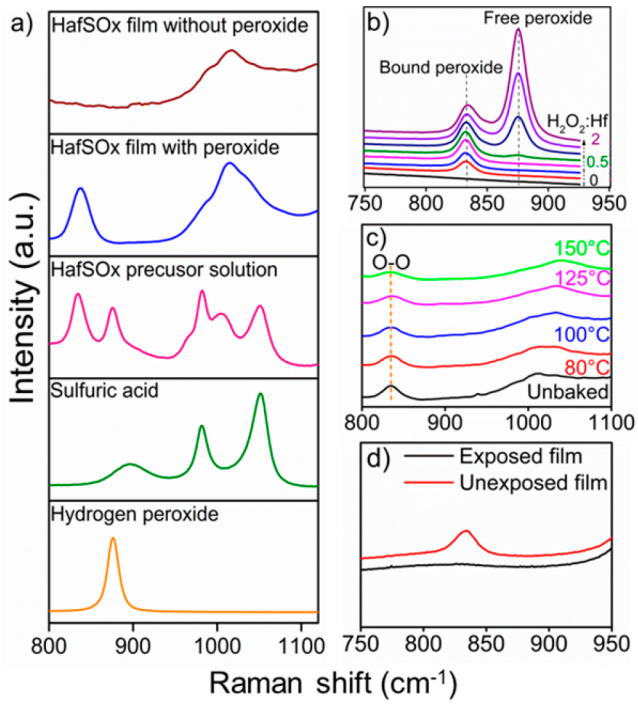

Figure 3. Raman analysis of HafSOx solutions and films. (a) Various precursor solution species and a film made with and without peroxide. (b) $HfOCl_2$ solutions containing peroxide to hafnium molar ratios ranging from 0 to 2. (c) Films heated at temperatures of 80 to 150 °C. (d) A film before and after electron beam exposure.

The ν(O−O) stretching mode in free (uncoordinated) peroxide appears at 876 cm^{-1} as seen in the spectrum for aqueous hydrogen peroxide. A new stretching mode is observed at 834 cm^{-1} for the HafSOx precursor solution, indicating that some of the peroxide was coordinated to hafnium.[36−38] The spectrum for sulfuric acid shows free sulfate and bisulfate symmetric stretching modes at 982 and 1050 cm^{-1}, respectively.[39] At least two additional stretching modes emerge for the HafSOx precursor solution with peaks at 967 and 1004 cm^{-1}. These modes can be assigned to sulfate that is coordinated to hafnium.[34,40,41] While the HafSOx precursor solution contains both free and bound forms of peroxide and sulfate, little to none of the free species are observed in the spin-coated films, suggesting nearly all of the sulfate and

DOI: 10.1021/acsanm.8b00865
ACS Appl. Nano Mater. 2018, 1, 4548−4556

Lam Research Ex. 1019 - Page 3
Lam Research Corp. v. Inpria Corp.
IPR2024-00033 - U.S. Patent No. 9,823,564

peroxide in the films are bound to hafnium. As expected, the Raman spectrum for HafSOx films formed with the peroxide free precursor does not have features related to peroxide.

As the radiation sensitive ligand, peroxide enables patterning in the HafSOx system. Therefore, the sensitivity of the final resist is likely related to the number of peroxide ligands that coordinate to each tetrameric Hf cluster. Figure 3b shows Raman spectra of $HfOCl_2$ solutions containing peroxide to hafnium ratios from 0 to 2. For peroxide to hafnium ratios <0.5, only the stretching mode at 834 cm^{-1} is observed, indicating that all of the peroxide coordinates to the clusters. When the peroxide to hafnium ratio exceeds 0.5, the free peroxide stretching mode at 876 cm^{-1} appears while the bound peroxide saturates in intensity. This suggests that approximately two peroxide groups coordinate to each hafnium tetramer. This is in agreement with previous studies which showed that two peroxide groups replace four hydroxyl groups to form the tetrameric species $[Hf_4(O_2)_2(OH)_4(H_2O)_{16}]^{8+}$.[42] Further studies were performed to determine the peroxide to hafnium ratio in the films. To do this, as deposited HafSOx films were etched from the substrate using tetramethylammonium hydroxide (TMAH). A molar ratio of peroxide to hafnium of 0.67 ± 0.09 was determined using a combination of permanganate titration and ICP-OES analysis. These results suggest peroxide binds to clusters at a rate of ∼2 peroxides per Hf tetramer, and the bound peroxide is completely retained in the HafSOx thin film after spin-coating the precursor solution.[25]

As deposited, the films exist in a gel-like state with clusters dispersed in a matrix of water. A modest postapplication bake (PAB) at ≈70−80 °C is required to drive off most of the water prior to radiation exposure. Ellipsometry measurements indicate that the film is reduced in thickness by approximately 10−15% during this process, suggesting that significant condensation and assembly of clusters has occurred. As the films are structurally amorphous at this stage (i.e., no long-range order was observed by electron or X-ray diffraction measurements), it is proposed that clusters assemble similar to what has been observed in the precursor solution.[34] That is, Hf tetramers containing ∼2 intracluster peroxide groups and 4 intracluster hydroxide groups are linked by intercluster sulfate groups. Because sulfate is present in the precursor solution at ratios of <1 sulfate per hafnium ion, charge balance considerations suggest that intercluster hydroxide groups also contribute to linking these clusters. Thus, HafSOx films in the exposure-ready condition may be visualized as a matrix of Hf cations, where peroxide is uniformly distributed on a sub-nanometer scale at a ratio of 1 peroxide per 2 hafnium ions, with sulfate and hydroxide competing for the remaining coordination sites and linking together the small clusters. While Hf−sulfate bonds in the material are thermally stable well above 70 °C,[43] Hf−hydroxide and Hf−peroxide are more susceptible to thermal decomposition. In particular, decomposition of Hf−peroxide during the PAB would eliminate the chemical contrast of the HafSOx thin film, and thus the thermal behavior of bound peroxide is critical to the function of the photoresist. To investigate this behavior, Raman spectra were acquired for films heated to several temperatures for 3 min as shown in Figure 3c. The peroxide group was found to be thermally stable in the films, with only a 20% decreased intensity after heating up to 125 °C and still present after heating up to 150 °C. Figure 3d shows Raman spectra for a HafSOx film after an 80 °C PAB and before and after exposure to a 5 keV electron beam with an 800 $\mu C/cm^2$ dose. The Raman peak associated with peroxide bound to hafnium is completely absent following electron beam exposure. These results indicate that the peroxide group is thermally stable but is readily eliminated by interaction with a 5 keV or 500 eV e-beam.[44] The separation of thermal and radiation peroxide decomposition is an important factor that enables HafSOx photoresists to function.

Following the PAB, the HafSOx film is ready for exposure to radiation and formation of a latent image. XPS was used to investigate the composition and chemical state of the HafSOx films after the PAB.Figure 4a shows an O 1s spectrum acquired after a long (>30 min) X-ray exposure.

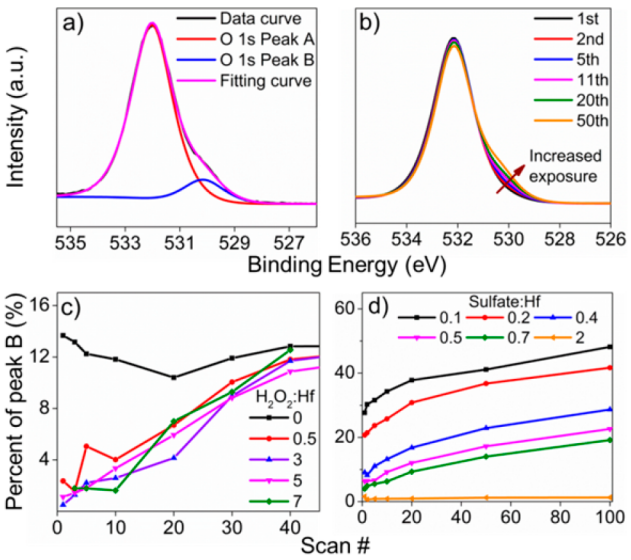

Figure 4. XPS analysis of HafSOx films. (a) O 1s spectrum of a film with a $HfOCl_2$:H_2O_2:H_2SO_4 precursor ratio of 1:3:0.7 acquired after a long (>30 min) X-ray exposure. (b) O 1s peak evolution of a HafSOx film for increasing X-ray exposure. (c) Evolution of the O 1s low binding energy peak area for films made with varying quantities of peroxide. (d) Evolution of the O 1s low binding energy peak area for films made with varying quantities of sulfate.

We found that the O 1s peak could be fit using two components. The higher binding energy (E_b) peak A (532.0 eV) is attributed to sulfate and hydroxyl groups.[43,45−48] The lower E_b peak B (530.2 eV) corresponds to a Hf−O−Hf oxide network, where this E_b is similar to what has been observed for hafnium oxides.[43,47−49] For an initial XPS spectrum with limited X-ray exposure, peak B was considerably smaller than what was observed in Figure 4a. To investigate this phenomenon, O 1s spectra were collected repeatedly from the same sample area of a HafSOx film, and the changes in the spectra are shown in Figure 4b. The lower E_b component is seen to increase in intensity with increasing X-rays exposure, which can be correlated to the development of an oxide network during exposure to X-ray radiation. Figure 4c shows the relative at. % of peak B of the total O 1s peak area in the HafSOx film, which enables a quantitative analysis of the dynamic formation of the oxide network. This analysis was performed for HafSOx films containing varying amounts of peroxide. HafSOx films without peroxide showed considerable oxide formation even for the first O 1s spectrum, with no increase in oxide network formation for increasing X-ray exposure. However, films made with peroxide show virtually no

DOI: 10.1021/acsanm.8b00865
ACS Appl. Nano Mater. 2018, 1, 4548−4556

Lam Research Ex. 1019 - Page 4
Lam Research Corp. v. Inpria Corp.
IPR2024-00033 - U.S. Patent No. 9,823,564

oxide network formation to start but had significant oxide network formation with increasing X-ray exposure. Because regions of HafSOx exposed to radiation become insoluble in the subsequent pattern development step (discussed further below), it may be deduced that the decomposition of Hf–peroxide bonds leads to the formation of a Hf–oxide network, which results in the insoluble HafSOx in exposed regions. These XPS results allow for the direct analysis of the chemical changes associated with the exposure step of the patterning process. Furthermore, films made with at least a 0.5 peroxide to hafnium ratio behave similarly with respect to oxide network formation, confirming that peroxide content in the films does not exceed ≈0.5 per hafnium ion. Peak B saturates at ≈30 scans, corresponding to a flux of order 10^{15}–10^{16} photons/cm^2 and an energy dose of ≈1 J/cm^2. However, peroxide decomposition leading to oxide formation is likely driven by secondary electrons generated in the material during exposure, rather than directly by the radiation source.[44] The dose required for similar chemical transformation during exposure to EUV photons (relative to X-rays) would be considerably lower due to the higher absorption cross section at these wavelengths.

Oxide formation during thermal and radiation exposure can also be controlled by the concentration of sulfate groups. Figure 4d shows the at. % of peak B of the total O 1s peak area for HafSOx films containing varying quantities of sulfate. HafSOx films with less sulfate show more oxygen coordinated as an oxide network at the beginning of X-ray exposure. Because little or none of the peroxide decomposes during the 70 °C PAB heat treatment (Figure 3c), it may be concluded that the increased oxide network that is present for films containing less sulfate is due to thermal recombination of hydroxyl species bound to Hf. All films made with a ratio of sulfate to hafnium <2 exhibit increased oxide network formation with increased X-ray exposure. The curves also exhibit comparable slopes, suggesting similar quantities of peroxide are present in these HafSOx films, and this peroxide controls oxide network formation for a wide range of sulfate concentrations. Because hydroxide and peroxide species lead to oxide network formation via thermal and radiative mechanisms, respectively, we propose that sulfate limits this oxide network formation simply by displacing these species.

Formation of the oxide network due to radiation exposure results in a decreased solubility of exposed regions when developed in basic solutions.[50] This solubility difference gives the material the chemical contrast necessary to function as a photoresist. However, as discussed above, oxide formation does not occur solely by radiative decomposition of peroxide and thus controlling oxide network formation in HafSOx films prior to exposure is critical to the overall patterning process. QCM was used to further understand how changes in processing and HafSOx composition influence oxide network formation and the corresponding film solubility. Films were deposited onto QCM crystals, and the mass change was tracked during film dissolution in TMAH.[51,52] Figure 5a shows the dissolution of films made with and without peroxide.

HafSOx films containing peroxide are considerably more soluble as indicated by the rapid mass loss, which confirms the role of peroxide in preventing oxide formation prior to exposure. The temperature of the PAB also affects the solubility, as shown in Figure 5b. The films switches from soluble to insoluble with a PAB temperature increase of only 20 °C. For films made with less sulfate (0.5 relative to Hf) this

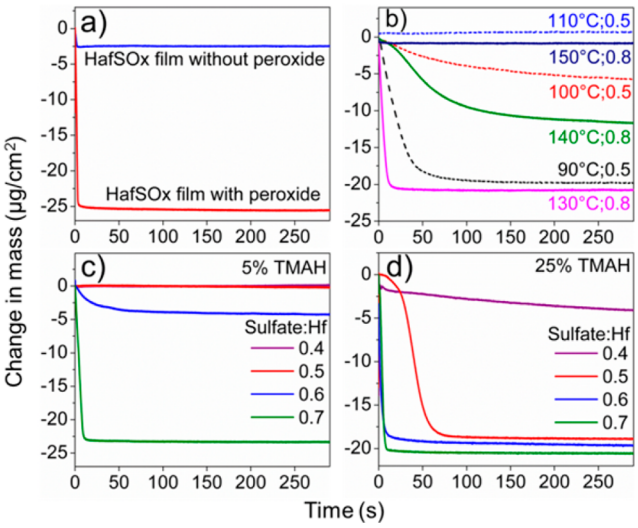

Figure 5. QCM measurements of HafSOx films dissolved in TMAH. (a) Films made with and without peroxide and a $HfOCl_2$:H_2O_2:H_2SO_4 ratio of 1:3:0.7 or 1:0:0.7, respectively, that were immersed in 5% TMAH. (b) Films made with a sulfate to Hf ratio of 0.5 and 0.8 heated to varying temperatures and immersed in 25% TMAH. (c) Films made with varying sulfate to Hf ratios immersed in 5% TMAH. (d) Films made with varying sulfate to Hf ratios immersed in 25% TMAH.

transition occurs at a lower temperature (i.e., 90–110 °C), whereas for films made with more sulfate (0.8 relative to Hf) the transition occurs at a higher temperature (i.e., 130–150 °C). Because sulfate replaces the hydroxide groups that lead to oxide network formation, more thermal energy is required to adequately form the oxide network at higher sulfate concentrations. The minimal thermal energy required to considerably decrease HafSOx solubility illustrates the potential for high sensitivity compared to other high-resolution resists.[19−21] Figures 5c and 5d show films made with varying quantities of sulfate. HafSOx films containing more sulfate etch faster, whereas films containing low sulfate to Hf ratios are virtually insoluble. These results are consistent with the XPS (Figure 4d), which indicates more extensive oxide network formation for low sulfate to hafnium ratios, and are consistent with the general solubility behavior of hafnium sulfate compounds. Neutral hafnium sulfates (containing no hydroxyl groups) such as $Hf(SO_4)_2{\cdot}nH_2O$ are largely soluble, whereas basic hafnium sulfates (containing hydroxyl groups) such as $Hf(OH)_2SO_4{\cdot}nH_2O$ are less soluble. Comparing Figures 5c with 5d also shows that films exhibit increased solubility in more concentrated TMAH.

In light of the above results, we now revisit the proposed chemical formula of HafSOx films, $Hf(O_2)_x(SO_4)_y(O)_z(OH)_{4-2x-2y-2z}{\cdot}qH_2O$, and consider the role of each species on the patterning mechanisms. By combining results from the above characterization methods, the stoichiometry of films made with varying amounts of sulfate was estimated using the following five constraints, and the results are summarized in Table 1: (1) Peroxide:Hf ratios were set to 0.5 based on Raman spectroscopy results. (2) Sulfate:Hf ratios were determined by S at. % and Hf at. % obtained by XPS. (3) Oxide:Hf ratios were determined by at. % peak B of the O 1s spectra obtained by XPS (i.e., the y-intercept in Figure 5d). (4) Hydroxide:Hf ratios were determined by charge balance and using the proposed chemical formula. (5)

DOI: 10.1021/acsanm.8b00865
ACS Appl. Nano Mater. 2018, 1, 4548−4556

Lam Research Ex. 1019 - Page 5
Lam Research Corp. v. Inpria Corp.
IPR2024-00033 - U.S. Patent No. 9,823,564

Table 1. Normalized at. % of Hf, O, and S Measured by XPS for HafSOx Films Made with Varying Sulfate:Hf Molar Ratios[a]

sulfate:Hf ratio in precursor solution	XPS atomic compositions			approximate stoichiometry	(sulfate + oxide):Hf
	Hf (%)	O (%)	S (%)		
0.10	23	74	3	$Hf(O_2)_{0.5}(SO_4)_{0.14}(O)_{0.90}(OH)_{0.92}\cdot H_2O_{-0.16}$	1.04
0.20	20	75	5	$Hf(O_2)_{0.5}(SO_4)_{0.25}(O)_{0.75}(OH)_{1.00}\cdot H_2O_{0.00}$	1.00
0.40	17	74	9	$Hf(O_2)_{0.5}(SO_4)_{0.51}(O)_{0.39}(OH)_{1.20}\cdot H_2O_{-0.28}$	0.90
0.50	16	73	11	$Hf(O_2)_{0.5}(SO_4)_{0.65}(O)_{0.27}(OH)_{1.15}\cdot H_2O_{-0.46}$	0.92
0.70	14	73	13	$Hf(O_2)_{0.5}(SO_4)_{0.86}(O)_{0.21}(OH)_{0.86}\cdot H_2O_{-0.30}$	1.07

[a]A corresponding film stoichiometry is approximated as described in the text.

Water:Hf ratios were determined using any signal from the O 1s spectra left unassigned after satisfying the above constraints.For all films, no excess oxygen (i.e., not assigned to the four anions) was required to satisfy the total atomic concentration measured by XPS. In considering the film stoichiometry in this way, the following relationships emerge. First, the sulfate content in the films can be directly controlled by the sulfate concentration in the precursor solution. This relationship is highly proportional (R^2 = 0.997), with ≈1.26 times more sulfate in films than the corresponding solution, suggesting clusters linked by sulfate groups in solution are preferentially retained upon spin-coating or segregate to the surface of the films. The role of sulfate in reducing oxide formation is illustrated clearly in the right-hand column of Table 1. For all films, the amount of sulfate + oxide is approximately constant (0.99 ± 0.07) with respect to Hf, and by extension, the amount of hydroxide with respect to Hf is also constant (1.03 ± 0.15). This suggests sulfate has displaced hydroxide groups that would have otherwise contributed to oxide formation. Furthermore, this hints at the possibility of a range of stabilities among Hf−hydroxide bonds in the material. That is, the most stable hydroxide groups are retained after film deposition and heating, independent of sulfate concentration. This procedure also led to negative coefficients for H_2O for most of the HafSOx films, suggesting little or no water was present, likely in part due to the ultrahigh vacuum environment of the XPS chamber or due to surface segregation of the sulfate groups which would lead to an overestimation of the amount of oxygen in the film.

The above results show that the solubility of HafSOx films is influenced by several variables including the addition of peroxide, sulfate content, PAB temperature, and TMAH concentration. Important photoresist parameters including resolution and sensitivity can also be controlled using these same variables. Figures 6a and 6b show SEM images of HafSOx arrays patterned using electron beam lithography.

The squares were patterned using an electron beam energy of 30 keV and a dose of 100−1500 $\mu C/cm^2$ with 40 $\mu C/cm^2$ increments. AFM thickness measurements of similar arrays were used to generate the contrast curve in Figure 6c. The films remain soluble at low doses, which can be seen by the lack of residual film in the SEM images at the top of Figures 6a and 6b and low normalized thickness in Figure 6c. The dose required to induce a solubility switch in the film (resist sensitivity) is controlled by varying the quantity of sulfate in the HafSOx photoresist. Films with lower sulfate concentrations (Figure 6a) more easily form a long-range oxide network and are thus more sensitive than films with higher sulfate concentrations (Figure 6b). However, this comes at the expense of decreased resolution, since areas adjacent to the exposed regions are more susceptible to oxide formation via proximity (electron scattering) effects. This is exemplified by

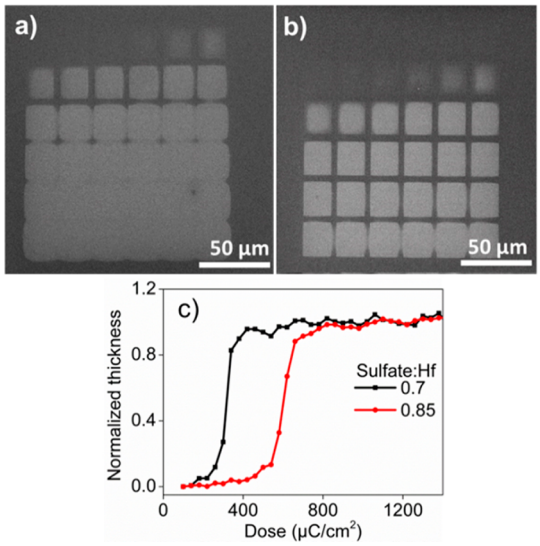

Figure 6. (a, b) SEM images of contrast arrays patterned using e-beam exposure doses of 100−1500 $\mu C/cm^2$ for HafSOx films made with sulfate to Hf ratios of (a) 0.7 and (b) 0.85. (c) Contrast curve produced from AFM analysis of similar contrast arrays.

the sharper edges observed for patterns formed from HafSOx with higher sulfate concentration (Figure 6b). These results are consistent with a lower image contrast for lower sulfate concentrations.

By the mechanisms described above, nanometer-sized patterns can be written using the HafSOx system. An example is shown in Figure 7, where a three-dimensional cross-hatch pattern was written using e-beam lithography.

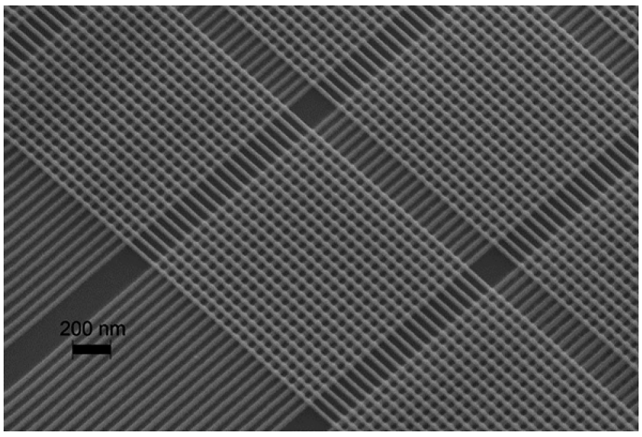

Figure 7. A three-dimensional pattern of HafSOx written using e-beam lithography with line widths and spacings of ≈30 nm at a dose of 500 $\mu C/cm^2$.

DOI: 10.1021/acsanm.8b00865
ACS Appl. Nano Mater. 2018, 1, 4548−4556

Lam Research Ex. 1019 - Page 6
Lam Research Corp. v. Inpria Corp.
IPR2024-00033 - U.S. Patent No. 9,823,564

This cross-hatched pattern was written using line widths and spacings (i.e., half-pitch) of ≈30 nm; however, patterning of features at <10 nm resolution has also been demonstrated for HafSOx and similar Hf-based resists using both e-beam[22] and EUV[24] lithography.

■ CONCLUSIONS

Metal oxo−hydroxo clusters offer a promising approach to patterning structures at lengths approaching the atomic scale. Beginning with these ultrasmall building blocks, careful selection of solution functionalizing species with consideration for the subsequent radiative and solubility requirements leads to the controlled assembly of clusters on film deposition and the generation of a photoresist. This was demonstrated with the aqueous-based HafSOx system. At each stage of the patterning process, metal−oxygen bonds are selectively formed by thermal and/or radiative energy as the material gradually transitions to an insoluble metal-oxide network. The extent of oxide formation is further controlled by the concentration of peroxide and sulfate in the precursor solution, and together these parameters drive key resist properties such as resolution and sensitivity. The nature of these transformations was monitored using several characterization techniques, and a fundamental understanding of the patterning mechanisms has emerged. Two limitations of HafSOx are the limited number of peroxide ligands that coordinate to hafnium and the moderate EUV absorption cross section of hafnium, which likely limit the sensitivity achievable using this photoresist. Metals capable of coordinating multiple peroxide groups (e.g., chromium, molybdenum, and tungsten) could enable improved sensitivity, while oxo−hydroxo photoresists with high EUV absorbers (e.g., tin, antimony, and bismuth) have already demonstrated increased sensitivity.

■ METHODS

Precursor Solution. A 1 M hafnium stock solution was produced by dissolving $HfOCl_2{\cdot}8H_2O$ (98+%; Alfa Aesar) in 18.2 MΩ water. The precise concentration of Hf was inferred by heating a small volume of solution to form pure HfO_2 and performing a gravimetrical analysis. Aqueous solutions of H_2SO_4 (1 M; BDH Chemicals) and H_2O_2 (30 wt %; Macron) were used as received. The HafSOx solutions were formed by sequential addition of $HfOCl_2$, H_2O_2, and H_2SO_4 followed by dilution with 18.2 MΩ water to achieve the desired concentration. A standard $HfOCl_2$:H_2O_2:H_2SO_4 ratio of 1:3:0.7 was used in all HafSOx film studies, unless otherwise noted. For other films with different ratios, the molar ratio of sulfate to hafnium ranged from 0.1 to 2. The molar ratio of peroxide to hafnium ranged from 0 to 7. The precursor solution molarity is defined relative to hafnium.

Film Deposition. For quartz crystal microbalance (QCM) experiments, films were deposited onto QCM crystals with SiOx coatings designed for liquid applications (Inficon). A hydrophilic surface was achieved prior to deposition using a UV/ozone treatment. Films used for Raman spectroscopy were deposited on sapphire or aluminum-coated SiO_2/Si substrates. All other films were deposited on native oxide Si (100) substrates. The Si substrates were rinsed sequentially using deionized water, acetone, and isopropanol, followed by a 5−10 min oxygen plasma treatment to achieve a hydrophilic surface. In all cases, the films were deposited by spin-coating for 30 s at 3000 rpm. After deposition, a PAB of 70−300 °C was applied by heating films on a hot plate.

Film Patterning. For e-beam lithography a $HfOCl_2$:H_2O_2:H_2SO_4 ratio of 1:3:0.68 precursor was spin-coated on a silicon substrate. A 30 keV electron beam was used to write parallel lines in the HafSOx layer, and the film was developed using 25% tetramethylammonium hydroxide (TMAH). A second HafSOx layer was spin-coated, and a 30 keV electron beam was used to write parallel lines perpendicular to the lines patterned in the first layer. The film was developed using 25% TMAH.

Dynamic Light Scattering (DLS). DLS analysis was done using a Mobiuζ instrument (Wyatt Technologies). The solutions were passed through a 0.1 μm PTFE syringe filter prior to measurements. Determination of the hydrodynamic radius and polydispersity was done using Dynamics software. Data were collected using a 5 s integration time and averaged over 20 measurements.

Spectroscopic Ellipsometry. Film thicknesses were measured with a J.A. Woolam variable angle spectroscopic ellipsometer using a Cauchy model. Data were collected from 400 to 1100 nm (10 nm steps) at incidence angles of 65° and 75°.

Microscopy. Transmission electron microscopy (TEM) images were taken at 200 kV with an FEI Titan 80−200 TEM. A surface functionalized TEM grid (NanoPlus, Dune Sciences) was used for imaging clusters from the precursor solution. The functionalized surface of the grid was placed on a droplet of 150 mM HafSOx solution and subsequently rinsed with deionized water to remove excess solution. For cross-sectional TEM images, a thin lamella was extracted from the HafSOx film using a focused ion beam on a Quanta 3D dual beam scanning electron microscope. Atomic force microscopy (AFM) analysis was performed with a Bruker Innova AFM in tapping mode. Silicon probes (Budget Sensors) were used at a 300 kHz resonance frequency and 40 N/m force constant. A polynomial background subtraction was applied to the images to correct for sample tilt and scanner bow. SEM images of contrast arrays were acquired at 5 kV using an FEI Nova NanoSEM 230.

Raman Spectroscopy. Liquid-phase Raman analysis (500−3000 cm^{-1}) was done with a Thermo Scientific DXR SmartRaman using a 780 nm laser. Thin film Raman analysis was done with a Horiba LabRAM 800 using a 532 nm laser, a 100× objective, and a 300 lines/mm grating. A SiO_2 standard was used to calibrate the Raman frequency shift.

Quartz Crystal Microbalance (QCM). Measurements of film dissolution rates were taken using a research quartz crystal microbalance (RQCM) and phase lock oscillator (PLO-10i) instrument (Inficon). A crystal holder designed for liquid contact was used to secure the QCM crystals. Crystals were submerged in high-purity (electronic grade) TMAH solutions (Alfa Aesar), and resonance frequency changes were measured using a frequency counter (Keithley). Custom software was used to record the data.

X-ray Photoelectron Spectroscopy (XPS). XPS analysis was done using a Thermo Scientific K-alpha X-ray photoelectron spectrometer equipped with a microfocused monochromatic Al Kα (1486.6 eV) X-ray source and ultralow energy electron flood gun. High-resolution spectra were acquired using a 50 eV pass energy. Avantage software (Thermo Scientific) was used to analyze the spectra. The binding energies were calibrated using the C 1s peak of adventitious carbon (284.8 eV). The number of O peaks was set to two, and peak full width half-maxima (fwhm) were constrained to be in the range 1.7−1.8 eV for peak fitting the O 1s spectra. The peak fitting was conducted with mixed Lorentzian and Gaussian peak shapes, while for background we used the "Smart" Shirley method.

Peroxide Analysis. Permanganate titrations were used to measure peroxide content in the films, while inductively coupled plasma optical emission spectrometry (ICP-OES) was used to measure hafnium content to determine the peroxide to Hf ratio. Films were removed from the Si substrates using 1 M sulfuric acid. Some of this solution was titrated with $KMnO_4$ while the rest was analyzed with a Teledyne Leeman Prodigy ICP-OES in axial mode using spectral lines of 277.33 and 239.33 nm. ICP-OES standards were produced using a 1000 ppm hafnium standard (Inorganic Ventures). All ICP-OES samples and standards were diluted using 1% nitric acid.

■ AUTHOR INFORMATION

Corresponding Authors

*(D.W.J.) E-mail dwj@uoregon.edu.
*(E.L.G.) E-mail garfunkel@chem.rutgers.edu.

DOI: 10.1021/acsanm.8b00865
ACS Appl. Nano Mater. 2018, 1, 4548−4556

Lam Research Ex. 1019 - Page 7
Lam Research Corp. v. Inpria Corp.
IPR2024-00033 - U.S. Patent No. 9,823,564

*(D.A.K.) E-mail douglas.keszler@oregonstate.edu.
*(G.S.H.) E-mail greg.herman@oregonstate.edu.

ORCID

Richard P. Oleksak: 0000-0003-4642-8152
Darren W. Johnson: 0000-0001-5967-5115
Douglas A. Keszler: 0000-0002-7112-1171
Gregory S. Herman: 0000-0002-7901-8451

Author Contributions

R.O., R.R., and F.L. contributed equally to this work.

Notes

The authors declare no competing financial interest.

■ ACKNOWLEDGMENTS

This material is based upon work in the Center for Sustainable Materials Chemistry, which is supported by the US National Science Foundation under Grant CHE-1606982, and the Semiconductor Research Corporation (Contract 2013-OJ-2438.001). D.W.J. is a Scialog Fellow of Research Corporation for Science Advancement.

■ REFERENCES

(1) Cronin, L.; Müller, A. From serendipity to design of polyoxometalates at the nanoscale, aesthetic beauty and applications. *Chem. Soc. Rev.* **2012**, *41*, 7333−7334.

(2) Thompson, L. F.; Willson, C. G.; Bowden, M. J. *Introduction to Microlithography*; American Chemical Society: Washington, DC, 1983.

(3) Gallatin, G. M.; Naulleau, P.; Niakoula, D.; Brainard, R.; Hassanein, E.; Matyi, R.; Thackeray, J.; Spear, K.; Dean, K. Resolution, LER, and sensitivity limitations of photoresists. In *SPIE Advanced Lithography*; International Society for Optics and Photonics: 2008; p 69211E.

(4) Ito, H.; Marty, J. D.; Mauzac, M. Chemical Amplification Resists for Microlithography. In *Microlithography/Molecular Imprinting*; Springer Science & Business Media: 2005; Vol. *172*, pp 37−245.

(5) Yasin, S.; Hasko, D.; Ahmed, H. Fabrication of < 5 nm Width Lines in Poly(methylmethacrylate) Resist Using a Water:Isopropyl Alcohol Developer and Ultrasonically-Assisted Development. *Appl. Phys. Lett.* **2001**, *78*, 2760−2762.

(6) Duan, H.; Winston, D.; Yang, J. K.; Cord, B. M.; Manfrinato, V. R.; Berggren, K. K. Sub-10-nm Half-Pitch Electron-Beam Lithography by Using Poly(methylmethacrylate) as a Negative Resist. *J. Vac. Sci. Technol., B: Nanotechnol. Microelectron.: Mater., Process., Meas., Phenom.* **2010**, *28*, C6C58−C6C62.

(7) Grigorescu, A.; Hagen, C. Resists for Sub-20-nm Electron Beam Lithography with a Focus on HSQ: State of the Art. *Nanotechnology* **2009**, *20*, 292001.

(8) Manfrinato, V. R.; Zhang, L.; Su, D.; Duan, H.; Hobbs, R. G.; Stach, E. A.; Berggren, K. K. Resolution Limits of Electron-Beam Lithography Toward the Atomic Scale. *Nano Lett.* **2013**, *13*, 1555−1558.

(9) Yoshimura, T.; Shiraishi, H.; Yamamoto, J.; Okazaki, S. Nano Edge Roughness in Polymer Resist Patterns. *Appl. Phys. Lett.* **1993**, *63*, 764−766.

(10) Nagase, M.; Namatsu, H.; Kurihara, K.; Iwadate, K.; Murase, K.; Makino, T. Nano-Scale Fluctuations in Electron Beam Resist Pattern Evaluated by Atomic Force Microscopy. *Microelectron. Eng.* **1996**, *30*, 419−422.

(11) Yamaguchi, T.; Namatsu, H.; Nagase, M.; Yamazaki, K.; Kurihara, K. Nanometer-Scale Linewidth Fluctuations Caused by Polymer Aggregates in Resist Films. *Appl. Phys. Lett.* **1997**, *71*, 2388−2390.

(12) Fujita, J.; Ohnishi, Y.; Ochiai, Y.; Matsui, S. Ultrahigh Resolution of Calixarene Negative Resist in Electron Beam Lithography. *Appl. Phys. Lett.* **1996**, *68*, 1297−1299.

(13) Dai, J.; Chang, S. W.; Hamad, A.; Yang, D.; Felix, N.; Ober, C. K. Molecular Glass Resists for High-Resolution Patterning. *Chem. Mater.* **2006**, *18*, 3404−3411.

(14) Namatsu, H.; Takahashi, Y.; Yamazaki, K.; Yamaguchi, T.; Nagase, M.; Kurihara, K. Three-Dimensional Siloxane Resist for the Formation of Nanopatterns with Minimum Linewidth Fluctuations. *J. Vac. Sci. Technol., B: Microelectron. Process. Phenom.* **1998**, *16*, 69−76.

(15) Trikeriotis, M.; Krysaki, M.; Chung, Y. S.; Ouyang, C.; Cardineau, B.; Brainard, R.; Ober, C. K.; Giannelis, E. P.; Cho, K. Nanoparticle Photoresists from HfO_2 and ZrO_2 for EUV Patterning. *J. Photopolym. Sci. Technol.* **2012**, *25*, 583−586.

(16) Li, L.; Liu, X.; Pal, S.; Wang, S.; Ober, C. K.; Giannelis, E. P. Extreme Ultraviolet Resist Materials for Sub-7 nm Patterning. *Chem. Soc. Rev.* **2017**, *46*, 4855−4866.

(17) Mojarad, N.; Gobrecht, J.; Ekinci, Y. Beyond EUV lithography: a comparative study of efficient photoresists' performance. *Sci. Rep.* **2015**, *5*, 9235.

(18) Anderson, J. T.; Munsee, C. L.; Hung, C. M.; Phung, T. M.; Herman, G. S.; Johnson, D. C.; Wager, J. F.; Keszler, D. A. Solution-Processed HafSOx and ZircSOx Inorganic Thin-Film Dielectrics and Nanolaminates. *Adv. Funct. Mater.* **2007**, *17*, 2117−2124.

(19) Stowers, J.; Keszler, D. A. High Resolution, High Sensitivity Inorganic Resists. *Microelectron. Eng.* **2009**, *86*, 730−733.

(20) Telecky, A.; Xie, P.; Stowers, J.; Grenville, A.; Smith, B.; Keszler, D. A. Photopatternable Inorganic Hardmask. *J. Vac. Sci. Technol., B: Nanotechnol. Microelectron.: Mater., Process., Meas., Phenom.* **2010**, *28*, C6S19−C6S22.

(21) Stowers, J. K.; Telecky, A.; Kocsis, M.; Clark, B. L.; Keszler, D. A.; Grenville, A.; Anderson, C. N.; Naulleau, P. P. Directly Patterned Inorganic Hardmask for EUV Lithography. In *SPIE Advanced Lithography*; International Society for Optics and Photonics: 2011; pp 796915−796915-11.

(22) Oleksak, R. P.; Ruther, R. E.; Luo, F.; Fairley, K. C.; Decker, S. R.; Stickle, W. F.; Johnson, D. W.; Garfunkel, E. L.; Herman, G. S.; Keszler, D. A. Chemical and Structural Investigation of High-Resolution Patterning with HafSOx. *ACS Appl. Mater. Interfaces* **2014**, *6*, 2917−2921.

(23) Fairley, K. C.; Sharps, M. C.; Mitchson, G.; Ditto, J.; Johnson, D. W.; Johnson, D. C. Sub-30 keV Patterning of HafSOx Resist: Effects of Voltage on Resolution, Contrast, and Sensitivity. *J. Vac. Sci. Technol., B: Nanotechnol. Microelectron.: Mater., Process., Meas., Phenom.* **2016**, *34*, 041607.

(24) Mojarad, N.; Hojeij, M.; Wang, L.; Gobrecht, J.; Ekinci, Y. Single-Digit-Resolution Nanopatterning with Extreme Ultraviolet Light for the 2.5 nm Technology Node and Beyond. *Nanoscale* **2015**, *7*, 4031−4037.

(25) Amador, J. M.; Decker, S. R.; Lucchini, S. E.; Ruther, R. E.; Keszler, D. A. Patterning Chemistry of HafSOx Resist. In *SPIE Advanced Lithography*; International Society for Optics and Photonics: 2014; pp 90511A−90511A-6.

(26) Frederick, R. T.; Amador, J. M.; Goberna-Ferron, S.; Nyman, M.; Keszler, D. A.; Herman, G. S. Mechanistic study of HafSOx extreme ultraviolet inorganic resists. *J. Phys. Chem. C* **2018**, *122*, 16100−16112.

(27) Kryask, M.; Trikeriotis, M.; Ouyang, C.; Chakrabarty, S.; Giannelis, E. P.; Ober, C. K. Nanoparticle Photoresists: Ligand Exchange as a New, Sensitive EUV Patterning Mechanism. *J. Photopolym. Sci. Technol.* **2013**, *26*, 659−664.

(28) Jiang, J.; Zhang, B.; Yu, M.; Li, L.; Neisser, M.; Chun, J. S.; Giannelis, E. P.; Ober, C. K. Oxide Nanoparticle EUV (ONE) Photoresists: Current Understanding of the Unusual Patterning Mechanism. *J. Photopolym. Sci. Technol.* **2015**, *28*, 515−518.

(29) Cardineau, B.; Del Re, R.; Marnell, M.; Al-Mashat, H.; Vockenhuber, M.; Ekinci, Y.; Sarma, C.; Freedman, D. A.; Brainard, R. L. Photolithographic Properties of Tin-Oxo Clusters Using Extreme Ultraviolet Light (13.5 nm). *Microelectron. Eng.* **2014**, *127*, 44−50.

(30) Passarelli, J.; Murphy, M.; Del Re, R.; Sortland, M.; Dousharm, L.; Vockenhuber, M.; Ekinci, Y.; Neisser, M.; Freedman, D. A.; Brainard, R. L. High-Sensitivity Molecular Organometallic Resist for

DOI: 10.1021/acsanm.8b00865
ACS Appl. Nano Mater. 2018, 1, 4548−4556

Lam Research Ex. 1019 - Page 8
Lam Research Corp. v. Inpria Corp.
IPR2024-00033 - U.S. Patent No. 9,823,564

EUV (MORE). In *SPIE Advanced Lithography*; International Society for Optics and Photonics: 2015; pp 94250T−94250T-13.
(31) Muha, G. M.; Vaughan, P. A. Structure of the Complex Ion in Aqueous Solutions of Zirconyl and Hafnyl Oxyhalides. *J. Chem. Phys.* **1960**, *33*, 194−199.
(32) Åberg, M. An X-Ray Investigation of Some Aqueous Zirconium (IV) Halide, a Hafnium (IV) Chloride, and Some Zirconium (IV) Perchlorate Solutions. *Acta Chem. Scand.* **1977**, *31*, 171−181.
(33) Connick, R. E.; McVey, W. H. The Aqueous Chemistry of Zirconium. *J. Am. Chem. Soc.* **1949**, *71*, 3182−3191.
(34) Ruther, R. E.; Baker, B. M.; Son, J.-H.; Casey, W. H.; Nyman, M. Hafnium Sulfate Prenucleation Clusters and the Hf_{18} Polyoxometalate Red Herring. *Inorg. Chem.* **2014**, *53*, 4234−4242.
(35) Oleksak, R.; Herman, G. Characterization of High-Resolution HafSOx Inorganic Resists. In *SPIE Advanced Lithography*; International Society for Optics and Photonics: 2014; pp 90483H−90483H-8.
(36) Dengel, A. C.; Griffith, W. P. Studies on Transition Metal Peroxo Complexes—IX. Carboxylato Peroxo Complexes of Niobium (V), Tantalum (V), Zirconium (IV) and Hafnium (IV). *Polyhedron* **1989**, *8*, 1371−1377.
(37) Tarafder, M.; Miah, M. L. Novel peroxo complexes of zirconium containing organic ligands. *Inorg. Chem.* **1986**, *25*, 2265−2268.
(38) Tarafder, M.; Bhattacharjee, P.; Sarkar, A. Peroxo Complexes of Chromium (VI), Molybdenum (VI), Tungsten (VI) and Zirconium (IV) Ions Containing Tridentate and Quadridentate Neutral Ligands. *Polyhedron* **1992**, *11*, 795−798.
(39) Malinowski, E. R.; Cox, R. A.; Haldna, U. L. Factor Analysis for Isolation of the Raman Spectra of Aqueous Sulfuric Acid Components. *Anal. Chem.* **1984**, *56*, 778−781.
(40) Rudolph, W. W.; Brooker, M. H.; Tremaine, P. R. Raman Spectroscopy of Aqueous $ZnSO_4$ Solutions Under Hydrothermal Conditions: Solubility, Hydrolysis, and Sulfate Ion Pairing. *J. Solution Chem.* **1999**, *28*, 621−630.
(41) Szilágyi, I.; Königsberger, E.; May, P. M. Characterization of Chemical Speciation of Titanyl Sulfate Solutions for Production of Titanium Dioxide Precipitates. *Inorg. Chem.* **2009**, *48*, 2200−2204.
(42) Thompson, R. C. Equilibrium Studies and Redox Kinetics of the Peroxo Complex of Zirconium (IV) in Acidic Perchlorate Solution. *Inorg. Chem.* **1985**, *24*, 3542−3547.
(43) Flynn, B.; Kim, D.; Clark, B. L.; Telecky, A.; Arnadottir, L.; Szanyi, J.; Keszler, D. A.; Herman, G. S. In-Situ Characterization of Aqueous-Based Hafnium Oxide Hydroxide Sulfate Thin Films. *Surf. Interface Anal.* **2014**, *46*, 210−215.
(44) Frederick, R. T.; Herman, G. S. Characterization of HafSOx Inorganic Photoresists Using Electron Stimulated Desorption. In *SPIE Advanced Lithography*; International Society for Optics and Photonics: 2016; pp 97790I−97790I-7.
(45) Vasquez, R. XPS Core Level Spectra of Some Y Compounds. *J. Electron Spectrosc. Relat. Phenom.* **1990**, *50*, 167−170.
(46) Colón, J. L.; Thakur, D. S.; Yang, C.-Y.; Clearfield, A.; Martini, C. R. X-Ray Photoelectron Spectroscopy and Catalytic Activity of α-Zirconium Phosphate and Zirconium Phosphate Sulfophenylphosphonate. *J. Catal.* **1990**, *124*, 148−159.
(47) Barreca, D.; Milanov, A.; Fischer, R. A.; Devi, A.; Tondello, E. Hafnium Oxide Thin Film Grown by ALD: An XPS Study. *Surf. Sci. Spectra* **2007**, *14*, 34−40.
(48) Shimizu, H.; Sato, T.; Konagai, S.; Ikeda, M.; Takahashi, T.; Nishide, T. Temperature-Programmed Desorption Analyses of Sol−Gel Deposited and Crystallized HfO_2 Films. *Jpn. J. Appl. Phys.* **2007**, *46*, 4209.
(49) Sarma, D.; Rao, C. XPES Studies of Oxides of Second- and Third-Row Transition Metals Including Rare Earths. *J. Electron Spectrosc. Relat. Phenom.* **1980**, *20*, 25−45.
(50) Telecky, A. J. Photoresist and Ion-Exchange Chemistry of HafSOx. Ph.D. Thesis, Oregon State University, Corvallis, OR, 2012.
(51) Hinsberg, W.; Willson, C.; Kanazawa, K. Measurement of Thin-Film Dissolution Kinetics Using a Quartz Crystal Microbalance. *J. Electrochem. Soc.* **1986**, *133*, 1448−1451.
(52) Hinsberg, W.; Houle, F.; Lee, S.-W.; Ito, H.; Kanazawa, K. Characterization of Reactive Dissolution and Swelling of Polymer Films Using a Quartz Crystal Microbalance and Visible and Infrared Reflectance Spectroscopy. *Macromolecules* **2005**, *38*, 1882−1898.

DOI: 10.1021/acsanm.8b00865
ACS Appl. Nano Mater. 2018, 1, 4548−4556

Lam Research Ex. 1019 - Page 9
Lam Research Corp. v. Inpria Corp.
IPR2024-00033 - U.S. Patent No. 9,823,564